Research Square

Preprints are preliminary reports that have not undergone peer review.
They should not be considered conclusive, used to inform clinical practice,
or referenced by the media as validated information.

Bio-inspired rebalancing through selective restraint loss

Anxin Guo

guoanxin@hit.edu.cn

Harbin Institute of Technology https://orcid.org/0000-0003-3464-9222

Jialei Yan

Harbin Institute of Technology

Ruicong Wu

Harbin Institute of Technology

Jiabin Liu

Harbin Institute of Technology

Chenchen Zhou

Harbin Institute of Technology

Hui li

Harbin Institute of Technology https://orcid.org/0000-0001-9198-3951

Article

Keywords:

Posted Date: November 26th, 2026

DOI: https://doi.org/10.21203/rs.3.rs-11751591/v1

License: This work is licensed under a Creative Commons Attribution 4.0 International License.
Read Full License

Additional Declarations: There is **NO** Competing Interest.

Bio-inspired rebalancing through selective restraint loss

Jialei Yan [1, #], Ruicong Wu [1, #], Jiabin Liu [1], Chenchen Zhou [1], Anxin Guo [1, *], Hui Li

[1] *Key Lab of Intelligent Monitoring and Early Warning for Transportation Infrastructure of the Ministry of Industry and Information Technology, School of Civil Engineering, Harbin Institute of Technology, Harbin 150090, China.*

ABSTRACT

Local restraint loss disrupts the force balance of distributed mooring systems, raising the question of whether further restraint reduction must increase the resulting displacement. Inspired by functional redistribution and arm autotomy in brittle stars, we propose a reconfiguration framework based on adjustment of surviving-line forces and spatially selected secondary restraint reduction. Experiments using a 1:70-scale floating bridge model and programmable pretension control show that additional slippage can partially compensate for the horizontal offset caused by an initial loss. Same-side combinations amplify the offset, whereas selected opposite-side combinations reduce it through redistribution of the remaining restoring forces. Horizontal departure therefore varies non-monotonically with affected-line count. Release sequence and inter-event interval shape the transient pathway, while configuration-dependent compensation persists under the tested regular-wave and combined wind–wave conditions. Smaller horizontal offsets can coexist with increased vertical motion or response variability. These findings establish spatially selected restraint reduction as a potential intervention for post-loss motion control and provide a mechanical basis for bio-inspired fault-tolerant reconfiguration of distributed mooring systems.

1. Introduction

Distributed restraint systems maintain equilibrium through forces transmitted at spatially separated connections. Local restraint loss changes the collective force and moment balance, displacing the supported body and redistributing loads among the surviving restraints. Research on damaged structures has shown that surviving components can develop alternative load paths and reorganize their mechanical contributions [1-4]. For a restrained floating system, this raises a control question: once an initial loss has produced a directional offset, can a further, spatially selected reduction in restraint partially counteract that offset? Answering this question would establish whether changes to the surviving restraint pattern can be used to influence post-loss motion.

Mooring systems provide a direct setting in which to examine this possibility [5]. Their restraint characteristics can change through line rupture [6, 7], fatigue-related degradation [8-11], anchor displacement [12-15], and interactions with the seabed [16-18]. Previous studies of single, multiple, and sequential mooring-line failures have established that failure location and line combination influence platform motion, surviving-line loads, and transient response [19-26].

# Jialei Yan and Ruicong Wu contributed equally to this work.

* Corresponding author.

E-mail address: guoanxin@hit.edu.cn.

These findings demonstrate that affected-line count alone is insufficient to describe the consequences of local loss. The control significance of this configuration dependence, however, requires further examination. In particular, a secondary restraint change acts on a system whose position and load distribution have already been altered by the first event. Whether that change reinforces or compensates for the existing offset depends on how it modifies the restoring actions of the remaining lines. Its location, order, and timing therefore offer potential means of directing the post-loss response.

Brittle stars provide biological inspiration for exploring these interventions. After arm loss, they can maintain locomotion by reassigning the roles and coordination of their surviving arms [27]. They also exhibit arm autotomy, changing the set of appendages available for subsequent coordination. Together, these features draw attention to both the contributions of surviving connections and the spatial pattern of connections that remain. Supporting evidence from harvestmen shows that different spatial patterns of appendage loss can produce different locomotor consequences even when the number of lost legs is unchanged [28]. The mechanical correspondence lies in distributed force transmission: brittle-star arms transmit substrate reaction forces to the central disc, whereas mooring lines transmit tensile forces to a floating body. This correspondence motivates two reconfiguration routes: adjusting the force contributions of surviving lines through controlled changes in effective length and pretension, and selectively reducing an additional restraint. A spatially selected secondary reduction intended to compensate for an existing offset is introduced here as an engineering hypothesis inspired by these biological features.

A multi-pontoon floating bridge provides an experimental realization of distributed mooring restraint [29-31]., coupling individual line tensions to the position and orientation of the floating structure. Previous studies highlight the coupled response arising from pontoon hydrodynamic interactions and hydroelasticity [32-34], alongside loading effects associated with spatially varying waves [35, 36] and wind–wave interactions [37-46]. This dependence on structural coupling and environmental forcing motivates testing whether spatial compensation persists under different loading conditions. We therefore compare wave, wind, and combined loading to determine whether configurations that amplify or compensate for the initial offset remain distinguishable.

Here, we investigate this hypothesis using a 1:70-scale floating bridge model and a calibrated, programmable equivalent pretension-release mechanism. We impose an initial single-line restraint loss followed by prescribed secondary slippage, varying the affected-line configuration, event order, and inter-event interval under regular-wave, wind-only, and combined wind–wave loading. We show that mean horizontal departure varies non-monotonically with affected-line count: selected secondary slippage events partially compensate for the offset caused by the initial loss. Spatial configuration governs the direction and extent of this compensation, while release sequence and interval shape its transient development. Configuration-dependent compensation remains evident in the tested combined wind–wave condition, although smaller horizontal offsets can coexist with increased vertical displacement or motion variability. These findings identify spatially selected restraint reduction as a potential intervention for bio-inspired post-loss motion control and

fault-tolerant mooring reconfiguration.

2. Results

Brittle-star-inspired post-damage mooring reconfiguration

Brittle stars combine flexible redistribution of arm function with the capacity for arm autotomy [27]. After losing an arm, they can continue moving by reassigning the roles and coordination of the surviving arms, without waiting for arm regeneration (Fig. 1a, b). They can also shed arms in response to predators or harmful stimuli [27]. Here, this capacity motivates the hypothesis of selective secondary release (Fig. 1c). Supporting evidence from harvestmen shows that losing two locomotor legs on the same side causes greater immediate locomotor impairment than bilateral loss [28], highlighting the importance of the spatial pattern of appendage loss. Together, these observations motivate the consideration of both functional redistribution and changes in the set of surviving connections.

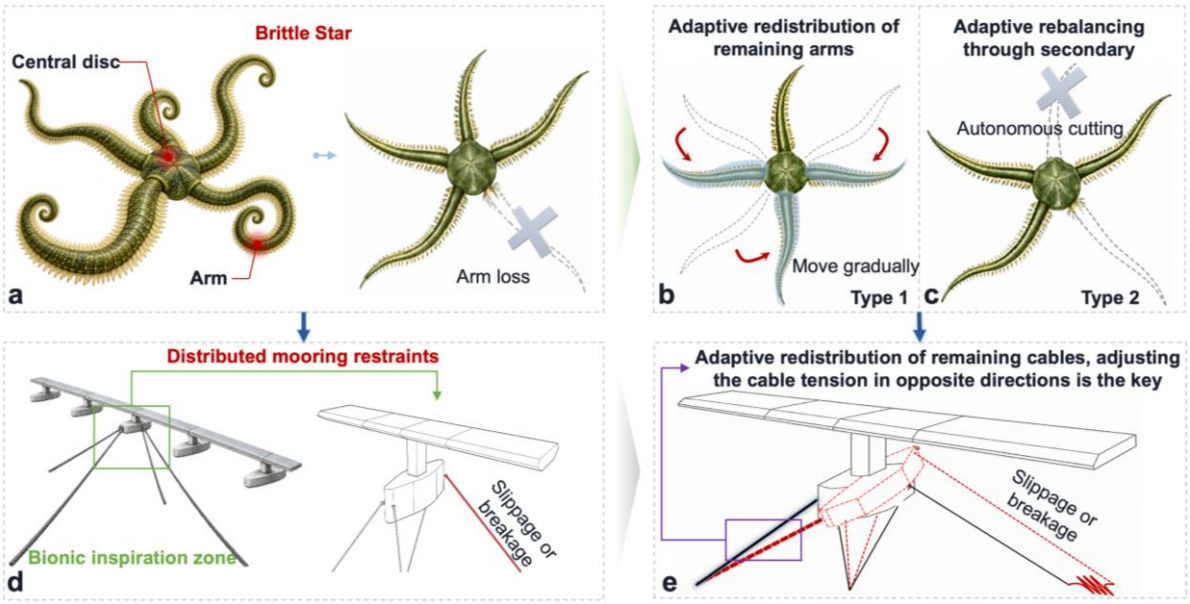

Fig. 1. Brittle-star-inspired mooring reconfiguration. a Brittle-star morphology and local arm loss. **b** Functional reassignment of remaining arms after damage. **c** Hypothetical secondary arm loss illustrating altered appendage configuration. **d** Mechanical analogy between brittle-star arms and distributed mooring restraints. **e** Bio-inspired secondary restraint release to redistribute restoring forces and potentially mitigate directional imbalance.

These observations suggest that the consequences of local loss depend on how the surviving connections transmit forces to the body. In brittle stars, arms transmit substrate reaction forces to the central disc; in a distributed mooring system, lines transmit tensile forces to a floating body through spatially distributed attachments (Fig. 1d). Arm loss is therefore mapped to local restraint loss, while the reorganization of surviving arms motivates adjustments to the relative mechanical contributions of the remaining lines. Each line contributes to the collective force and moment balance according to its tension, direction, and attachment location. Losing a loaded restraint disturbs this balance, linking a local change in force transmission to changes in the position and orientation of the floating body.

We translate these principles into two routes for modifying the post-loss equilibrium. In

the first, controlled cable slippage adjusts the effective lengths and associated tensions of selected surviving lines without releasing additional connections (Fig. 1e). In the second, an additional line is deliberately released at a prescribed location, changing the spatial pattern of active restraints. The question extends beyond how many lines lose restraint. We examine which lines most strongly influence floating-body equilibrium and how their relative positions shape their collective contribution. We further test how release locations, sequence and time intervals affect the transient response, and whether release history also changes the equilibrium ultimately reached. The subsequent experiments test whether these interventions can produce the proposed spatial rebalancing in a distributed mooring system.

Equivalent representation of mooring-line slippage

To impose controlled changes in mooring restraint, we modeled the tension reduction from line slippage using programmable spring-release assemblies (Fig. 2a, d, e). At a given structural configuration, an increase in effective mooring length reduces the tensile restraint provided by the affected line, changing its contribution to the collective force and moment balance. We therefore defined the equivalent representation in terms of the change in transmitted line tension. A motor-driven slider adjusted the spring deformation, while a load cell recorded the resulting tension. The spring force–deformation relationship was calibrated, and release-validation tests compared the achieved tension reductions and actual initiation times with their prescribed values. These measurements established the relationship between the imposed slider motion and the resulting change in restraint.

The system was implemented on a 1:70-scale, three-pontoon floating-bridge model tested in a wind–wave flume (Fig. 2b, c). The central and two side pontoons were connected by the bridge girder. Mooring lines passed through fixed underwater turning points and connected to the spring-release assemblies above the water surface (Fig. 2f). The turning points defined the local line directions, while the spring assemblies established the initial tensions and compliant restraint. Together with buoyancy, weight, and applied loads, the mooring forces governed the force and moment balance of the model. Each assembly could be actuated independently, allowing selected restraints to be modified while the coupled structural response was measured.

The model dynamics and mooring geometry are summarized in Fig. 2g, h. The measured horizontal and vertical bending-mode periods were 3.86 s and 0.86 s, respectively. Under Froude time scaling, these correspond to nominal prototype-scale periods of 32.3 s and 7.2 s. Figure 2h defines the pontoon geometry, loading direction, and numbering of the four mooring lines, providing a common reference for comparing different spatial patterns of restraint loss. The affected lines, slider displacements, and initiation times were prescribed for each test, enabling control over the location, magnitude, sequence, and intervals of restraint changes. Tests included single-line events, same-side and opposite-side paired configurations, four-line events, and sequential events under regular-wave, wind-only, and combined wind–wave loading. Structural motion and mooring-line tension were recorded synchronously to quantify changes in mean position, response fluctuations, low-frequency motion, and load redistribution. These measurements enabled the effects of restraint location and release history to be examined within the same experimental system.

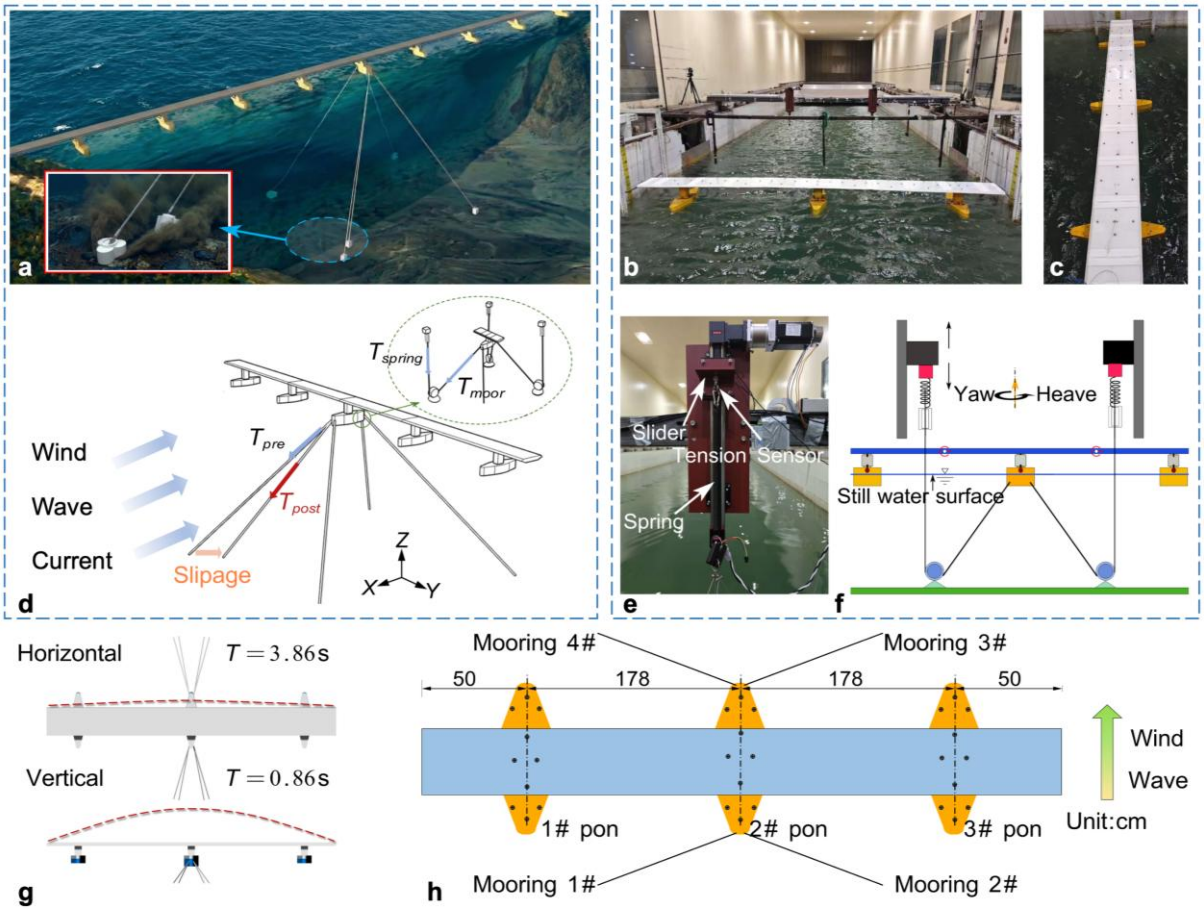

Fig. 2. Experimental framework for controlled mooring-restraint loss and secondary release. a Representative multi-pontoon floating bridge with distributed mooring restraint and a local slippage event. **b** Overview of the 1:70-scale three-pontoon model in the wind–wave flume. **c** Top view of the three-pontoon model. **d** Schematic of the principal forces and the change in mooring restraint associated with slippage. **e** Programmable pretension-release device comprising a slider, an equivalent spring, and a load cell. **f** Equivalent mooring arrangement of the scaled model. **g** Representative horizontal- and vertical-bending mode shapes. **h** Plan-view model geometry showing pontoon spacing, mooring-line numbering, and loading direction.

Single-line restraint loss produces location-dependent mean offsets

We first examined how the location of a single restraint loss affects post-slip re-equilibration. With the affected line count fixed at one, front-side Line 1 and rear-side Line 4 slippage produced opposing horizontal mean offsets under otherwise matched conditions (Fig. 3). Following the slip-induced transition, wave-driven oscillations continued around a shifted mean position (Fig. 3d, e). Line 1 slippage displaced the central pontoon predominantly towards negative X, whereas Line 4 slippage shifted it towards positive X. The corresponding X–Z trajectories showed that trajectory shape and oscillation envelope varied with wave period, while the opposing horizontal offsets remained evident across the tested conditions (Fig. 3a, b).

The displacement changes were accompanied by distinct patterns of mooring-tension redistribution (Fig. 3f). Tension in the affected line decreased rapidly, while the surviving

lines adjusted to different post-slip tension levels. The redistribution differed between Line 1 and Line 4 slippage, linking the location-dependent displacement response to changes in the collective restraint provided by the remaining lines. Changes in the steady post-slip mean and standard deviation, evaluated relative to the corresponding intact condition, quantified these differences (Fig. 3g). Line 1 slippage generally produced a larger absolute change in mean horizontal position than Line 4 slippage. Changes in response variability also depended on the affected line, wave period, and pontoon location. The central and side pontoons exhibited different combinations of mean displacement and variability changes, indicating that local restraint loss affected the spatial distribution of the response as well as its overall offset.

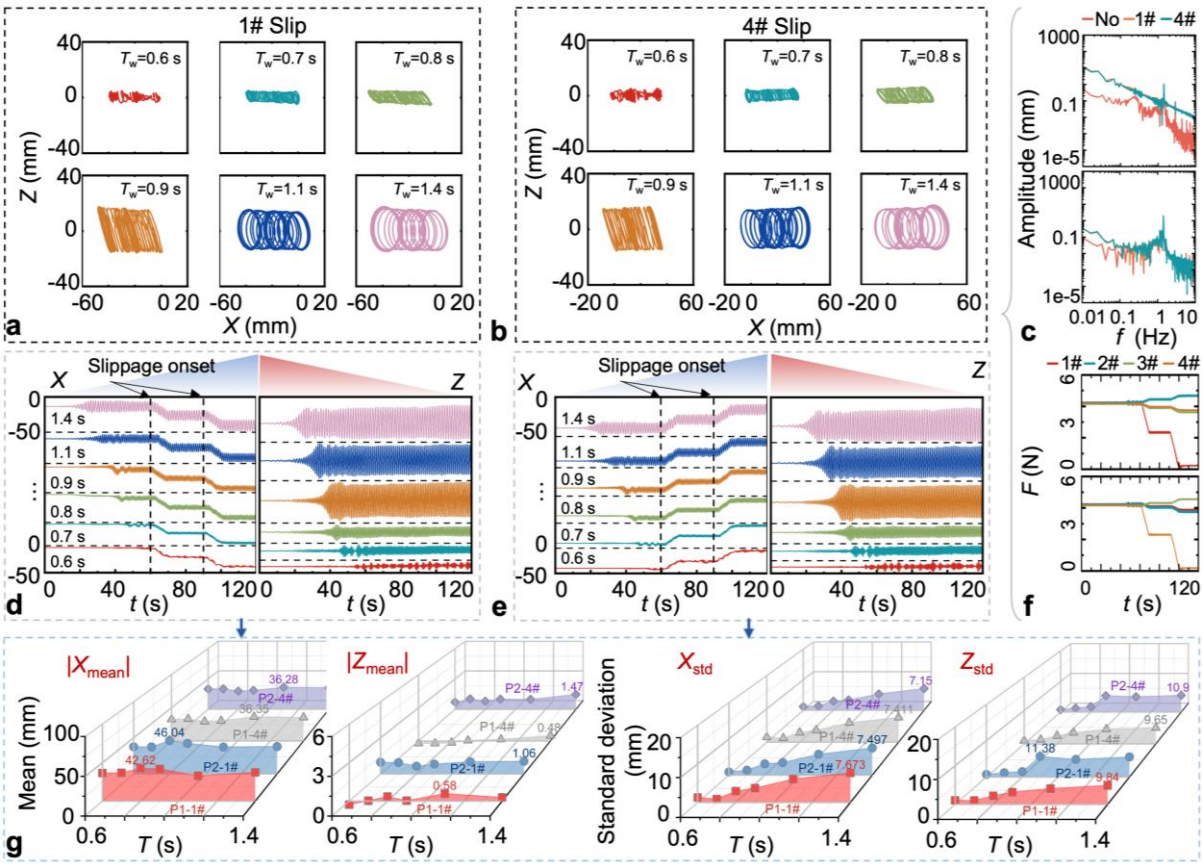

Fig. 3. Location-dependent response to single-line mooring slippage under regular waves. **a, b** *X*–*Z* trajectories of the center pontoon under different wave periods for front-side Line 1 and rear-side Line 4 slippage, respectively. **c** Amplitude spectra of the corresponding intact condition and the two single-line slippage cases. **d, e** *X*- and *Z*-direction displacement histories for Line 1 and Line 4 slippage, respectively. **f** Mooring-line tension evolution and redistribution following single-line slippage. **g** Changes in the mean and standard deviation of the *X*- and *Z*-direction displacements relative to the corresponding intact condition for the center and side pontoons across the tested wave periods.

Spectra calculated from the complete displacement records, including the slip transient, showed increased low-frequency content relative to the intact condition (Fig. 3c). These spectra characterize the complete event, including the transition in mean position; they do not isolate sustained post-slip oscillations. The wave-related peaks remained close to the imposed excitation frequency. Together, the displacement and tension measurements establish distinct post-slip states associated with the location of the first restraint loss. These states provide the

starting conditions for testing whether a subsequent restraint change amplifies the disturbance or redirects the resulting re-equilibration.

Selective secondary slippage counteracts the initial offset

We tested whether a spatially selected second slippage event could counteract the offset generated by the first restraint loss. Under regular-wave excitation, paired-line cases with the same affected-line count produced markedly different mean offsets (Fig. 4a, c). Same-side sequences 12 and 43 generated the largest shifts in opposing directions, whereas configurations 13, 14, 31, and 41 produced smaller offsets relative to the corresponding single-line cases. Here, sequence *ij* denotes slippage of Line *i* followed by Line *j*. The second event could therefore partially compensate for the initial displacement, even though an additional restraint was weakened.

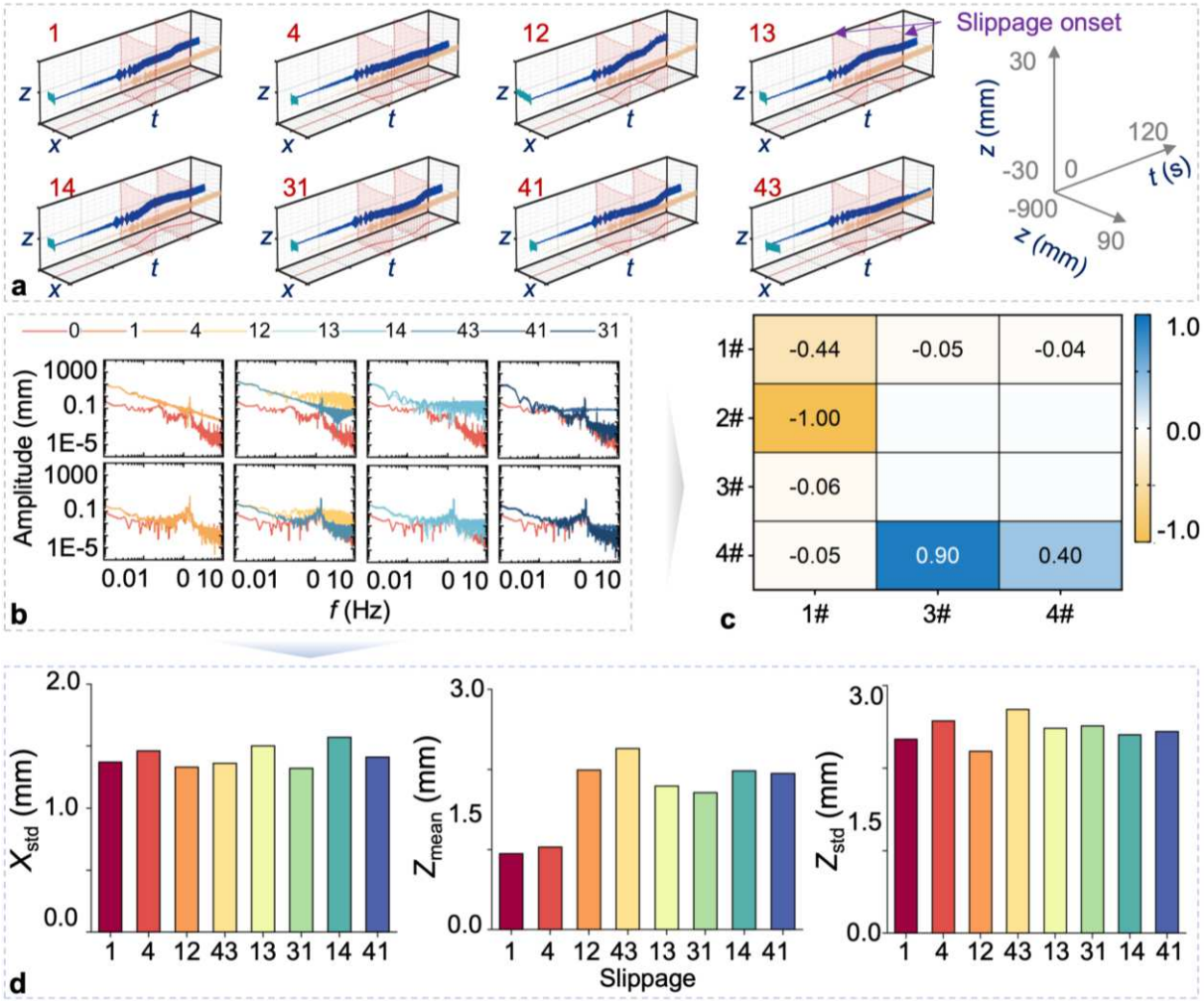

Fig. 4. Selective secondary slippage counteracts the initial offset. **a** Displacement time histories for single-line slippage and sequential paired-line slippage under regular waves. Sequence *ij* denotes slippage of Line *i* followed by Line *j*. Red planes indicate slippage initiation. **b** Displacement spectra for the intact, single-line, and paired-line cases. **c** Signed normalized mean horizontal shifts for the tested release configurations, showing the dependence of offset compensation on the identities of the affected lines. Blank cells denote untested combinations. Shifts were normalized by the maximum absolute shift across configurations. **d** Comparison of horizontal displacement standard deviation, mean vertical

displacement, and vertical displacement standard deviation across the tested configurations.

This compensation provides experimental support for the selective-release hypothesis introduced in Fig. 1c. Its mechanical connection to functional redistribution is that modifying a selected surviving restraint changes the collective restoring action available to the floating body. The paired-line comparisons show that the resulting horizontal position depends strongly on which restraints are modified and their relative spatial arrangement. Thus, the spatial-rebalancing principle proposed from biological inspiration can be realized as a reduction in post-loss horizontal mean offset in the distributed mooring system. Release order affected the transition between restraint states. Reversed sequences 13/31 and 14/41 followed different intermediate trajectories but approached similar final horizontal mean offsets under the tested conditions (Fig. 4a, c). For these comparisons, the spatial combination of affected lines was more influential on the final horizontal offset, while their order shaped the observed transient pathway.

The compensation was specific to the horizontal mean response. The vertical mean-response metric generally increased in paired-line cases, while horizontal and vertical variability differed among configurations (Fig. 4d). A smaller horizontal offset therefore did not imply simultaneous improvement in every response component. The spectra retained peaks near the imposed wave frequency, while low-frequency spectral content differed among configurations (Fig. 4b). Together, these results identify selective secondary restraint reduction as a means of redirecting post-loss re-equilibration, with its benefit depending on the response component being considered.

Spatially selective offset compensation persists under combined wind–wave loading

We next tested whether the configuration-dependent compensation observed under regular waves remained evident under combined wind–wave loading. The comparison was conducted at a wave height of 2.8 cm, a wave period of 0.7 s, and a wind speed of 3.5 m/s. Under this condition, same-side sequences 12 and 43 produced the largest negative and positive mean horizontal shifts, respectively, relative to their pre-slip positions, whereas configurations 13, 31, 14, and 41 produced smaller absolute shifts (Fig. 5c). Thus, adding a spatially selected second slippage event did not necessarily increase the displacement generated by the first. The offset-compensating behavior identified under regular waves remained observable in the tested combined-loading condition.

At a fixed wave height of 2.8 cm and period of 0.7 s, increasing wind speed altered the intensity and temporal distribution of the response associated with Line 1 slippage (Fig. 5a, b). Higher wind speeds produced more pronounced time-localized response features, most clearly at 6.5 m/s, while wave-related components remained evident in both the horizontal and vertical directions. The two directions exhibited different patterns of temporal modulation, showing that the effect of wind was dependent on the motion component. Wind loading modified the response intensity and intermittency, while the periodic wave excitation continued to organize the wave-related motion. The low-frequency features also contain the slip-induced transition in mean position and cannot be attributed entirely to sustained oscillations. These results establish the loading-dependent response characteristics against which spatial compensation among different slippage configurations is assessed in Fig. 5c.

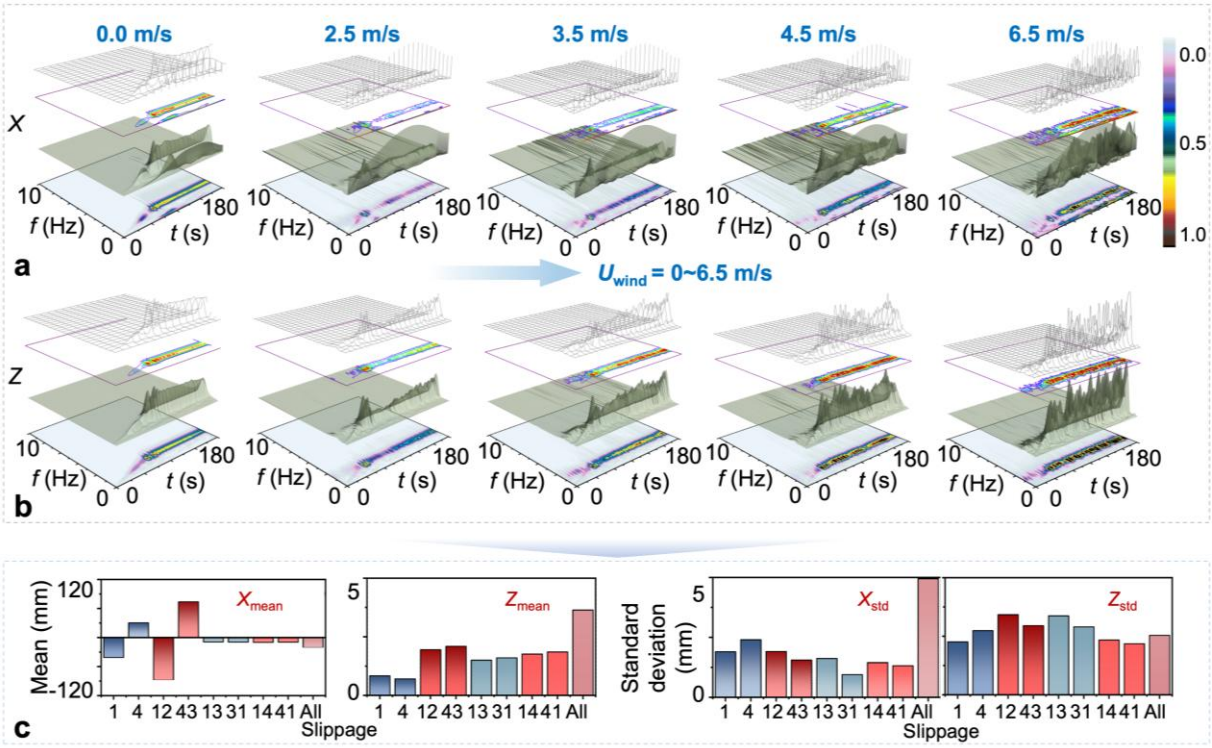

Fig. 5. Selective offset compensation and response variability under combined wind–wave loading. a, b Time–frequency representations of the X- and Z-direction displacement responses, respectively, at wind speeds of 0, 2.5, 3.5, 4.5, and 6.5 m/s. The corresponding pre-slip mean was subtracted from each displacement record before analysis. **c** Displacement statistics for the tested slippage configurations at U=3.5 m/s and T=0.7 s. From left to right: change in mean horizontal displacement, change in mean vertical displacement, horizontal displacement standard deviation, and vertical displacement standard deviation. Mean changes are defined relative to the corresponding pre-slip means; standard deviations characterize the post-slip analysis interval. "All" denotes slippage of all four lines.

The compensation was specific to the response component considered. Four-line slippage produced a smaller absolute mean horizontal shift than the same-side pairs, but the largest horizontal standard deviation and the largest magnitude of mean vertical shift (Fig. 5c). Reducing the horizontal offset therefore did not ensure simultaneous reductions in vertical displacement or motion variability. Together, these results support the selective-release hypothesis introduced in Fig. 1: changing the spatial pattern of restraint reduction can partially counteract a loss-induced horizontal offset, even under combined wind–wave loading. The persistence of this behaviour across the regular-wave and tested wind–wave conditions extends the evidence for spatial rebalancing, while retaining the trade-offs among mean position and response variability.

Release timing controls the transient pathway of rebalancing

Changing the inter-event interval altered the intermediate horizontal response while producing broadly comparable late-time mean positions for each ordered line pair (Fig. 6a). The first slippage event occurred at a common prescribed time, and the second followed after an interval of $\Delta t = t_2 - t_1 = 0$, 5, 10, 15, or 30 s. Simultaneous slippage produced a combined transition without an intermediate single-line stage. Increasing the interval separated the two

displacement changes and prolonged the response to the first restraint reduction before the second was introduced.

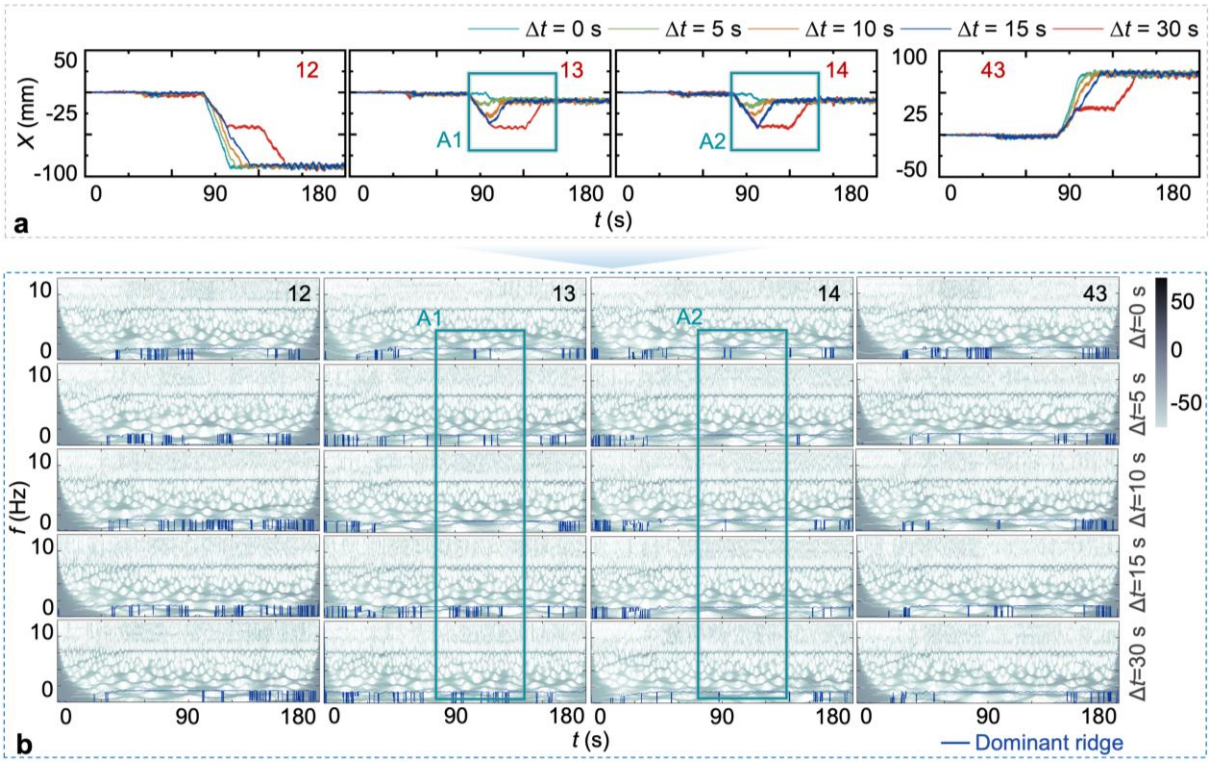

Fig. 6. Release timing controls the transient pathway of horizontal rebalancing. a X-direction displacement history for ordered slippage sequences 12, 13, 14, and 43 under regular waves, with inter-event intervals of Δt = 0, 5, 10, 15, and 30 s. Here, $\Delta t = t_2 - t_1$, where t_1 and t_2 denote the initiation times of the first and second slippage events, respectively; $\Delta t = 0$ denotes simultaneous slippage. Sequence *ij* denotes slippage of Line *i* followed by Line *j*. **b** Corresponding time-frequency representations of the *X*-direction displacement. Columns show sequences 12, 13, 14, and 43, and rows show increasing inter-event intervals from top to bottom. Blue curves indicate the extracted dominant ridges. Regions A1 and A2 identify the intermediate horizontal excursions associated with sequences 13 and 14, respectively.

The consequence of this delay depended on the spatial relationship between the affected lines. For same-side sequences 12 and 43, the second event extended the horizontal displacement initiated by the first. For sequences 13 and 14, it redirected the response towards a smaller horizontal offset. Longer intervals allowed the initial offset to persist before this compensating change occurred, whereas shorter intervals brought the opposing displacement changes closer together in time. Release timing therefore controlled the duration and evolution of the intermediate offset, while the selected line pair determined whether the second event reinforced or counteracted the first.

The dominant ridges reveal how release timing reorganized the horizontal response during spatial compensation (Fig. 6b). Within regions A1 and A2 for sequences 13 and 14, the ridges temporarily shifted towards very low frequencies during the intermediate horizontal excursion. Longer inter-event intervals, most clearly at Δt = 30 s, extended this low-frequency segment before wave-related frequency tracking reappeared following the compensating transition. Shorter intervals brought these changes closer together in time. This

correspondence links the ridge evolution to the displacement histories: delaying the second slippage event prolonged the intermediate offset, whereas introducing it earlier brought forward the compensating response. The low-frequency ridge segments characterize the slow displacement transition rather than establishing a new oscillatory mode. Together, the ridge and displacement changes show that spatially selected secondary slippage redirects the horizontal response, while its timing regulates the duration of the intermediate state.

Taken together with the preceding configuration comparisons, these results demonstrate a brittle-star-inspired route to horizontal rebalancing through spatially selected restraint reduction. A second slippage event can redirect force redistribution and partially compensate for the offset generated by the first; its timing controls how that compensation unfolds. Within the tested conditions, the spatial arrangement of the affected lines governed the direction of the mean-position change, while release sequence and inter-event interval shaped the transient pathway. Post-loss reconfiguration therefore provides a means of controlling both the horizontal offset and the evolution of the response through the choice and timing of restraint changes.

3. Discussion

Inspired by functional redistribution and arm autotomy in brittle stars, we propose post-loss mooring reconfiguration through controlled adjustment of surviving-line forces and spatially selected secondary restraint reduction. The central finding is that weakening an additional restraint can partially compensate for the horizontal offset caused by an initial local loss. The relationship between affected-line count and horizontal departure is therefore non-monotonic in the tested configurations. This establishes a basis for using selected restraint reduction to redirect post-loss motion through changes in the collective force and moment balance.

Calibrated experiments demonstrated that the outcome depended on the spatial relationship between successive restraint changes. Same-side slippage amplified the initial horizontal departure, whereas selected opposite-side combinations partially counteracted it. Release sequence and inter-event interval shaped the transient pathway, with broadly comparable late-time mean horizontal positions reached for a given affected-line pair. The distinction between offset-amplifying and offset-compensating configurations persisted in the tested combined wind–wave condition, supporting the applicability of spatial rebalancing across the loading conditions examined. Smaller horizontal offsets nevertheless coexisted with greater vertical displacement or motion variability in some configurations, revealing the response trade-offs associated with reconfiguration.

These findings identify spatially selected restraint reduction as a potential control action for fault-tolerant distributed mooring systems. They provide an experimental basis for managing post-loss motion through the location, magnitude, and timing of restraint adjustment. The broader implication is that the spatial organization of surviving restraints can be deliberately used to compensate for selected consequences of local loss, providing a basis for bio-inspired position and attitude control.

Future research can build on this principle to develop adaptive mooring systems that

coordinate restraint adjustment in response to local loss and changing environmental loads. Such systems would use the spatial distribution of surviving restraints as a control resource, extending the present findings towards fault-tolerant position and attitude control.

4. Methods

Experimental facility

Experiments were performed in the wind–wave flume facility at Harbin Institute of Technology, China. The facility comprises a recirculating wind tunnel integrated with a wave flume, enabling controlled wave, wind, and combined wind–wave loading. The test section measures 50.0 m in length, 6.0 m in width, and 3.6 m in height. Regular waves were generated by a flap-type wavemaker installed at one end of the flume, while an absorbing beach at the opposite end was used to minimize wave reflection. The still-water depth was 2.1 m.

Scaled floating bridge model

A 1:70-scale floating-bridge model was designed to represent a prototype bridge with a total length of 320 m. To preserve the dominant dynamic characteristics of the moored floating system while maintaining experimental feasibility, a representative three-pontoon subsystem centered on the moored pontoon was selected. The pontoons and piers were fabricated from 2-mm-thick aluminum plates, and ballast was added to achieve the target mass distribution and center of gravity. The main girder adopted a hybrid configuration comprising an internal load-bearing member and an external transparent acrylic fairing. The internal member was designed to satisfy the scaled sectional stiffness requirements. In contrast, the acrylic fairing reproduced the target external geometry and enabled effective wind-load transfer without introducing appreciable additional stiffness to the primary load-bearing system.

Equivalent force-based representation of mooring-line slippage

The mooring system was simplified as four symmetrically arranged mooring lines connected to the central pontoon. Each line was redirected by a fixed pulley near the bottom of the flume and then connected in series with an equivalent spring and a tension load cell. This arrangement enabled direct measurement of line tension and controlled simulation of slippage-induced pretension loss.

In the prototype system, local anchor or seabed slippage modifies the mooring geometry. It reduces the effective restoring capacity, which is manifested mechanically as a release of mooring pretension and a redistribution of line tension. In the present experiments, this consequence was not reproduced by directly imposing geometric sliding of the anchor. Instead, mooring-line slippage was represented through an equivalent force-based mapping using a computer-controlled slider system. The load cell was mounted on a carriage moving along a vertical guide rail driven by a synchronous-belt linear stage with a travel range of 0.40 m. By prescribing the carriage displacement, the deformation of the equivalent spring and the corresponding line tension could be adjusted in a repeatable manner, thereby reproducing partial or complete pretension release associated with localized mooring slippage.

Around the pre-slippage operating point, the tension change induced by prototype

slippage can be approximated by a local tangent relation,

$$\Delta T_{\mathrm{pro}} = -K_m \Delta L_{\mathrm{slip}} \tag{1}$$

where ΔT_{pro} is the tension change in the prototype mooring line, K_m is the equivalent tangent stiffness of the mooring system near the operating point, and ΔL_{slip} is the effective mooring-length increment associated with prototype slippage.

In the experimental system, the equivalent mooring tension is expressed as

$$T_{\mathrm{exp}}(t) = k_{\mathrm{eq}} \left[\delta_0 + u_m(t) - s(t) \right] \tag{2}$$

where $T_{exp}(t)$ is the equivalent experimental tension, k_{eq} is the equivalent stiffness of the slider–spring system, δ_0 is the initial spring extension associated with pretension, $u_m(t)$ is the deformation increment induced by structural motion, and $s(t)$ is the prescribed slider displacement. The corresponding tension change caused by a slider displacement increment Δs is

$$\Delta T_{\mathrm{exp}} = -k_{\mathrm{eq}} \Delta s \tag{3}$$

The experimental representation was established by matching the tension release in the equivalent system to the mechanical consequence of prototype slippage, namely,

$$\Delta T_{\mathrm{exp}} = \Delta T_{\mathrm{pro}} \tag{4}$$

which yields

$$k_{\mathrm{eq}} \Delta s = K_m \Delta L_{\mathrm{slip}} \tag{5}$$

This formulation indicates that the present method does not directly attempt to reproduce the full geometric evolution of anchor sliding. Instead, it reproduces the mechanically equivalent consequence of slippage, namely the reduction in effective restoring force and the associated redistribution of mooring tension. Partial slippage corresponds to a prescribed slider displacement smaller than the pre-slippage spring extension. In contrast, complete slippage is approached when the prescribed release reduces the equivalent line tension to approximately zero.

Instrumentation and data acquisition

Hydrodynamic and structural responses were measured using synchronized wave, motion, acceleration, and tension acquisition systems. Wave gauges recorded the free-surface elevation at 1000 Hz. The motions of the floating bridge model were captured using a Qualisys Track Manager motion-capture system at 150 Hz. Accelerometers measured structural accelerations at 1000 Hz, and mooring-line tensions were recorded by load cells at 1000 Hz. These synchronized measurements were used to quantify the transition from local tension loss to changes in global structural response.

Test matrix

The test matrix included intact-mooring and prescribed-slippage cases under wave-only, wind-only, and combined wind–wave conditions. Regular wave cases were examined over

representative wave periods of 0.6, 0.7, 0.8, 0.9, 1.1, and 1.4 s. Combined wind–wave tests were further conducted at increasing wind speeds. Owing to the symmetry of the structural configuration and mooring layout, the slippage combinations were reduced to representative scenarios: single-line slippage, same-side paired-line, opposite-side paired-line slippage, and four-line slippage. Representative cases included Line 1, Line 4, Lines 1+2, Lines 4+3, Lines 1+3, Lines 3+1, Lines 1+4, and Lines 4+1. For selected cases, a prescribed time lag between two slippage events was introduced to investigate the influence of slippage timing on the cascade process.

Data processing and response indicators

The response signals were analyzed in both the time and frequency domains. For each test, the pre-slippage and post-slippage segments were extracted from the full time-history records of pontoon displacement, acceleration, and mooring tension. The changes in mean displacement and mean tension were used to quantify slippage-induced offsets and load release. In contrast, the response standard deviation was used to characterize the amplification of oscillatory motion. Frequency-domain analyses were performed using the fast Fourier transform to identify changes in dominant response components and the enhancement of low-frequency energy after slippage. Time–frequency analyses were further conducted to track the temporal evolution of dominant-frequency ridges and the redistribution of response energy during the slippage process. Based on these analyses, the severity of each slippage scenario was evaluated using a set of indicators, including the mean response step change, standard deviation, low-frequency energy ratio, and tension redistribution magnitude.

Data availability

The data supporting the findings of this study are available within the article, its Supplementary Information and the accompanying Source Data file. Additional information is available from the corresponding authors upon reasonable request.

References

1. Reyes-Suárez, J. C. *et al.* Latent resistance mechanisms of steel truss bridges after critical failures. *Nature* **645**, 101-107 (2025).
2. Setiawan, A. *et al.* Breaking continuity to prevent catastrophic building collapse. *Nat. Commun.* **17**, 7546 (2026).
3. Moreno, R., Faíña, A., Sudhakaran, S., Walker, K. & Risi, S. Smart cellular bricks for decentralized shape classification and damage recovery. *Nat. Commun.* **17**, 5932 (2026).
4. Ozaki, T., Ohta, N. & Fujiyoshi, M. Self-rerouting sensor network for electronic skin resilient to severe damage. *Nat. Commun.* **16**, 1196 (2025).
5. Shu, H., Yao, A., Ma, K.-T., Ma, W. & Miller, J. API RP 2SK 4th edition—an updated stationkeeping standard for the global offshore environment. in Offshore Technology Conference, Houston, Texas, USA, 2018).
6. Chuang, Z., Chang, X., Li, C., Lu, Y. & Liu, S. Performance change of a semi-submersible production platform system with broken mooring line or riser. *Eng. Fail. Anal.* **118**, 104819 (2020).

7. Jia, W. *et al.* Investigation of barge-type FOWT in the context of concurrent and cascading failures within the mooring systems. *Renew. Energy* **224**, 120119 (2024).
8. Dai, J., Leira, B. J., Moan, T. & Alsos, H. S. Effect of wave inhomogeneity on fatigue damage of mooring lines of a side-anchored floating bridge. *Ocean Eng.* **219**, 108304 (2021).
9. Perez, I. M., Constantinescu, A., Bastid, P., Zhang, Y.-H. & Venugopal, V. Computational fatigue assessment of mooring chains under tension loading. *Eng. Fail. Anal.* **106**, 104043 (2019).
10. Leong, D., Low, Y. M. & Kim, Y. Control variates for efficient long-term extreme analysis of mooring lines. *Eng. Struct.* **221**, 111063 (2020).
11. Sun, K. *et al.* Dynamic response analysis of floating wind turbine platform in local fatigue of mooring. *Renew. Energy* **204**, 733-749 (2023).
12. Aubeny, C. & Chi, C. Mechanics of drag embedment anchors in a soft seabed. *J. Geotech. Geoenviron. Eng.* **136**, 57-68 (2010).
13. Zhang, W., Zhou, Z., Pradhan, D. L., Wang, P. & Jin, H. Design considerations of drag anchors in cohesive soil for floating facilities in the South China sea. *Mar. Struct.* **81**, 103101 (2022).
14. Lai, Y., Huang, Y., Gilbert, R. B. & Aubeny, C. P. Behavior of piggy-backed drag embedment anchors in marine soils. *J. Geotech. Geoenviron. Eng.* **148**, 04021167 (2022).
15. Chen, H., Gao, Y., Shu, S. & Lai, Y. The six-degree-of-freedom behavior of drag embedment anchor installed in clay. *Ships Offshore Struct.* **19**, 461-470 (2024).
16. Rui, S. *et al.* Analysis of mooring system for floating wind turbine based on macro-model of chain-seabed interaction. *Mar. Struct.* **104**, 103877 (2025).
17. Xiong, L., Yang, J. & Zhao, W. Dynamics of a taut mooring line accounting for the embedded anchor chains. *Ocean Eng.* **121**, 403-413 (2016).
18. Koh, K. X., Kim, Y. & Hossain, M. S. Cyclic response of a stiffened suction caisson anchor in calcareous silt. *Ocean Eng.* **201**, 107097 (2020).
19. Qiao, D. *et al.* Transient responses evaluation of FPSO with different failure scenarios of mooring lines. *J. Mar. Sci. Eng.* **9**, 103 (2021).
20. Zhang, Z., Wang, X., Zhang, X., Zhou, C. & Wang, X. Dynamic responses and mooring line failure analysis of the fully submersible platform for floating wind turbine under typhoon. *Eng. Struct.* **301**, 117334 (2024).
21. Jia, W., Yue, M., Miao, W., Yang, Y. & Li, C. Dynamic analysis of a 5 MW Barge-type FOWT with two-mooring failure of wind-wave misalignment scenarios. *Ocean Eng.* **285**, 115456 (2023).
22. Ren, Y., Shi, W., Venugopal, V., Zhang, L. & Li, X. Experimental study of tendon failure analysis for a TLP floating offshore wind turbine. *Appl. Energy* **358**, 122633 (2024).
23. Li, Y. *et al.* Effects of mooring line fracture on 15 MW floating offshore wind turbine under different operation strategies. *Eng. Fail. Anal.* **179**, 109754 (2025).
24. Wu, J. *et al.* A Markov resilience assessment framework for tension leg platform under mooring failure. *Reliab. Eng. Syst. Saf.* **231**, 108939 (2023).

25. Wu, J., Yu, Y., Cheng, S., Li, Z. & Yu, J. Probabilistic multilevel robustness assessment framework for a TLP under mooring failure considering uncertainties. *Reliab. Eng. Syst. Saf.* **223**, 108458 (2022).
26. Lu, Z.-Q. *et al.* Ocean wave energy harvesting with high energy density and self-powered monitoring system. *Nat. Commun.* **15**, 6513 (2024).
27. Kano, T. *et al.* A brittle star-like robot capable of immediately adapting to unexpected physical damage. *R. Soc. Open Sci.* **4**, 171200 (2017).
28. Escalante, I., Badger, M. A. & Elias, D. O. Rapid recovery of locomotor performance after leg loss in harvestmen. *Sci. Rep.* **10**, 13747 (2020).
29. Ma, K.-T., Luo, Y., Kwan, C.-T. T. & Wu, Y. *Mooring system engineering for offshore structures*. (Gulf Professional Publishing, 2019).
30. Domínguez, J. M. *et al.* SPH simulation of floating structures with moorings. *Coast. Eng.* **153**, 103560 (2019).
31. Jiang, Z. Mooring design for floating wind turbines: A review. *Renew. Sustain. Energy Rev.* **212**, 115231 (2025).
32. Yan, J. L., Wu, R. C., Yuan, X. W., Liu, J. B. & Guo, A. X. Diffraction and radiation effects of the multi-body pontoon system under the combination of earthquakes and waves. *Earthq. Eng. Struct. Dyn.* **54**, 2265-2282 (2025).
33. Fenerci, A., Kvåle, K. A., Xiang, X. & Øiseth, O. Hydrodynamic interaction of floating bridge pontoons and its effect on the bridge dynamic responses. *Mar. Struct.* **83**, 103174 (2022).
34. Viuff, T., Ravinthrakumar, S., Økland, O. D., Grytå, O. A. & Xiang, X. Model test of a hydroelastic truncated floating bridge with a stay-cable tower. *Appl. Ocean Res.* **135**, 103539 (2023).
35. Xiang, S., Cheng, B., Tang, M. & Abdelbaset, H. Effects of spatial inhomogeneity of wave excitations on structural behaviors of multi-span floating bridges. *Ocean Eng.* **243**, 110340 (2022).
36. Cheng, Z., Gao, Z. & Moan, T. Wave load effect analysis of a floating bridge in a fjord considering inhomogeneous wave conditions. *Eng. Struct.* **163**, 197-214 (2018).
37. McAllister, M. *et al.* Three-dimensional wave breaking. *Nature* **633**, 601-607 (2024).
38. Buckley, M. P., Horstmann, J., Savelyev, I. & Carpenter, J. R. Direct observations of airflow separation over ocean surface waves. *Nat. Commun.* **16**, 5526 (2025).
39. Olfateh, M., Ware, P., Callaghan, D., Nielsen, P. & Baldock, T. Momentum transfer under laboratory wind waves. *Coast. Eng.* **121**, 255-264 (2017).
40. Sullivan, P. P. & McWilliams, J. C. Dynamics of winds and currents coupled to surface waves. *Annu. Rev. Fluid Mech.* **42**, 19-42 (2010).
41. da Costa, B. M., Wang, J., Jakobsen, J. B., Snæbjörnsson, J. þ. & Øiseth, O. A. Long-term response of a curved floating bridge to inhomogeneous wind fields. *J. Wind Eng. Ind. Aerodyn.* **240**, 105488 (2023).
42. Viuff, T., Ravinthrakumar, S., Økland, O. D., Grytå, O. A. & Xiang, X. Experimental study of floating bridge global response when subjected to waves and current. *Appl. Ocean Res.* **138**, 103588 (2023).

43. Wu, R. C., Guo, A. X., Zhu, S. J. & Liu, J. B. Growth of wind-driven waves under uniform currents. *Coast. Eng.* **198**, 104704 (2025).
44. Chiapponi, L., Addona, F., Diaz-Carrasco, P., Losada, M. & Longo, S. Statistical analysis of the interaction between wind-waves and currents during early wave generation. *Coast. Eng.* **159**, 103672 (2020).
45. Kumar, K. & Shemer, L. Laboratory study of the effect of mean water current on the evolution of young wind waves. *J. Fluid Mech.* **996**, A21 (2024).
46. Escobar, A., Baker, J., Guillard, F., Faug, T. & Einav, I. Experimental confirmation of secondary flows within granular media. *Nat. Commun.* **16**, 7446 (2025).

Funding

This work was supported by the National Natural Science Foundation of China (Grant Nos. 52438009, 52595691, 52508546, and 523B2087), the China Postdoctoral Science Foundation (2025M774325), the Postdoctoral Fellowship Program (Grade B) of China Postdoctoral Science Foundation (GZB20250977), and the Heilongjiang Graduate Excellence Funding Program (LJYXLZR2025-011).

Author contributions

A.G., H.L., J.Y., and R.W. conceived the study. J.Y. and R.W. developed the methodology, conducted the experiments, analyzed the data, prepared the figures, and wrote the original manuscript. J.L. and C.Z. contributed to the experimental setup, data acquisition, and validation. A.G. and H.L. supervised the study, provided resources, acquired funding, and critically revised the manuscript. All authors discussed the results, reviewed the manuscript, and approved the submitted version.

Competing interests

The authors declare no competing interests.

Supplementary Files

This is a list of supplementary files associated with this preprint. Click to download.

- Supplementary.docx
- data.xlsx